

Temperature dependent terahertz giant anisotropy and cycloidal spin wave modes in $BiFeO_3$ single crystal

Fan Liu(刘凡), Zuanming Jin(金钻明), Xiumei Liu(刘秀梅), Yuqing Fang(方雨青), Jiajia Guo(国家嘉), Yan Peng(彭滟), Zhenxiang Cheng(程振祥), Guohong Ma(马国宏), Yiming Zhu(朱亦鸣)

Citation: Chin. Phys. B . 2020, 29(7): 077804 . **doi:** 10.1088/1674-1056/ab8dae
Journal homepage: http://cpb.iphy.ac.cn; http://iopscience.iop.org/cpb

What follows is a list of articles you may be interested in

Single-shot measurement of THz pulses

Lei Yang(杨磊), Lei Hou(侯磊), Chengang Dong(董陈岗), Wei Shi(施卫)
Chin. Phys. B . 2020, 29(5): 057803 . **doi:** 10.1088/1674-1056/ab821f

Graphene's photonic and optoelectronic properties-A review

A J Wirth-Lima, P P Alves-Sousa, W Bezerra-Fraga
Chin. Phys. B . 2020, 29(3): 037801 . **doi:** 10.1088/1674-1056/ab5fc2

Effects of deposition temperature on optical properties of MgF_2 over-coated Al mirrors in the VUV

Chun Guo(郭春), Bin-Cheng Li(李斌成), Ming-Dong Kong(孔明东), Da-Wei Lin(林大伟)
Chin. Phys. B . 2019, 28(11): 117801 . **doi:** 10.1088/1674-1056/ab457a

Review of ultrafast spectroscopy studies of valley carrier dynamics in two-dimensional semiconducting transition metal dichalcogenides

Dong Sun(孙栋), Jia-Wei Lai(赖佳伟), Jun-Chao Ma(马骏超), Qin-Sheng Wang(王钦生), Jing Liu (刘晶)
Chin. Phys. B . 2017, 26(3): 037801 . **doi:** 10.1088/1674-1056/26/3/037801

Selective excitation of molecular mode in a mixture by femtosecond resonance-enhanced coherent anti-Stokes Raman scattering spectroscopy

He Ping,Li Si-Ning,Fan Rong-Wei,Li Xiao-Hui,Xia Yuan-Qin,Yu Xin,Chen De-Ying
Chin. Phys. B . 2012, 21(2): 027801 . **doi:** 10.1088/1674-1056/21/2/027801

SPECIAL TOPIC — Terahertz physics

Temperature dependent terahertz giant anisotropy and cycloidal spin wave modes in $BiFeO_3$ single crystal*

Fan Liu(刘凡)[1], Zuanming Jin(金钻明)[1,2,5,†], Xiumei Liu(刘秀梅)[2], Yuqing Fang(方雨青)[1], Jiajia Guo(国家嘉)[2], Yan Peng(彭滟)[1,5], Zhenxiang Cheng(程振祥)[3], Guohong Ma(马国宏)[2,4,‡], and Yiming Zhu(朱亦鸣)[1,5,§]

[1] *Shanghai Key Laboratory of Modern Optical System, and Engineering Research Center of Optical Instrument and System (Ministry of Education), University of Shanghai for Science and Technology, Shanghai* 200093, *China*

[2] *Department of Physics, Shanghai University, Shanghai* 200444, *China*

[3] *Institute for Superconducting and Electronic Materials, University of Wollongong, NSW, Australia*

[4] *SIOM & STU Joint Laboratory for Superintense Lasers and the Applications, Shanghai* 201210, *China*

[5] *Shanghai Institute of Intelligent Science and Technology, Tongji University, Shanghai* 200092, *China*

(Received 29 March 2020; revised manuscript received 21 April 2020; accepted manuscript online 28 April 2020)

THz time-domain spectroscopy (THz-TDS) is used to study the THz-optical properties of a single crystal bismuth ferrite $BiFeO_3$ (BFO). It can be found that the anisotropy of $BiFeO_3$ is strongly dependent on the temperature. A giant birefringence up to around 3.6 is observed at 1 THz. The presence of a spatially modulated cycloidal antiferromagnetic structure leads to spin cycloid resonances (SCR) ψ and Φ, corresponding to the out-of-plane and in-plane modes of the spin cycloid, respectively. We distinguish the SCR with respect to their response to orthogonal polarizations of the electric fields of the incident THz beam. In addition, we observe a resonance appearing below 140 K, which might be interpreted as an electromagnon mode and related to a spin reorientation transition. Our present observations present that the temperature and polarization, as the external control parameters, can be used to modulate the THz optical properties of BFO single crystal.

Keywords: time resolved terahertz spectroscopy, dielectric anisotropy, spin cycloid resonance

PACS: 78.47.J–, 78.20.–e, 76.50.+g, 75.30.Ds **DOI:** 10.1088/1674-1056/ab8dae

Multiferroic materials combine ferroelectricity with magnetism and have been the platform of fascinating physical phenomena and functionalities. $BiFeO_3$ (BFO) is a ferroelectric (FE) G-type antiferromagnetic material at room temperature. The Néel temperature of BFO is about 640 K, and the ferroelectric Curie temperature is about 1100 K.[1–3] The crystal of BFO is a rhombohedrally distorted perovskite.[4] The electrical polarization $\boldsymbol{P}$ in BFO crystal is along the pseudocubic [111] direction. Note that the optical axis of the BFO crystal is parallel to $\boldsymbol{P}$. The Dzyaloshinskii–Moriya interaction (DM) $\boldsymbol{D}$ along $[-1, 2, -1]$ rotates the antiferromagnetic vector, forming a spin cycloid with a long modulation period of 62 nm in the $(-1, 2, -1)$ plane.[5]

Plenty of optical properties have been investigated, such as photovoltaic effect,[6,7] photo-stiction,[8] coherent acoustic phonons,[9,10] structural dependent ultrafast electron–phonon coupling[11] as well as nonlinear optical properties of BFO films and crystals.[12] THz coherent wave can be generated from BFO by ultrashort laser excitation via optical rectification.[13] THz emission spectroscopy has been used in FE domain imaging and optical readout of the state of FE memories of BFO.[14] Note that spin modes in BFO were under investigation in recent years using either inelastic neutron scattering,[15,16] Raman scattering spectroscopy,[17,18] far-infrared Fourier spectroscopy,[19,20] or RF technology.[21]

Recently, the excitations of high frequency magnetic resonance modes $\psi_1^{(1,2)}$ and $\varphi_2^{(1,2)}$ in polycrystalline BFO were studied at frequencies of 0.49–0.77 THz with a vector network analyzer-based spectrometer.[22] Although such enticing sub-THz spin cycloid resonances can be demonstrated by only the continuous wave absorption spectroscopy,[23,24] the THz frequency-resolved optical properties of the BFO crystal have not been reported sufficiently. The multiferroic materials are promising for quite a number of applications in the THz spectral range. For example, the BFO crystal shows the strong unidirectional transmission over the GHz–THz frequency range.[25] BFO thin film on $SrTiO_3$ shows a large amplitude modulation in the nonlinear optical response and

*Project supported by the National Natural Science Foundation of China (Grant Nos. 61975110, 11674213, 61735010, and 11604202), the 111 Project, China (Grant No. D18014), the International Joint Lab Program supported by Science and Technology Commission Shanghai Municipality, China (Grant No. 17590750300), the Key Project supported by Science and Technology Commission Shanghai Municipality, China (Grant No. YDZX20193100004960), Science and Technology Commission of Shanghai Municipality, China (Shanghai Rising-Star Program 18QA1401700), and Shanghai Educational Development Foundation, China (Chen Guang Project 16CG45).

†Corresponding author. E-mail: physics_jzm@usst.edu.cn

‡Corresponding author. E-mail: ghma@staff.shu.edu.cn

§Corresponding author. E-mail: ymzhu@usst.edu.cn

© 2020 Chinese Physical Society and IOP Publishing Ltd

ferroelectric polarization gated by THz fields, which points toward ferroelectric photonic switches and electromechanical devices.[26] BFO/Si and BFO/ZnO heterojunctions can be used to manipulate the THz radiation.[27,28] Recently, domain-wall engineered BFO thin films offer the prospects for bias-free strong THz emitters.[29] Hence, for such practical applications, the comprehensive characterization of the polarization- and temperature-dependent dielectric properties and the low-energy spin-dynamics of the BFO crystal at THz regime is required.

In this paper, we not only report the giant birefringence and dichroism by using THz time-domain spectroscopy (THz-TDS) in the frequency region of 0.4–1.2 THz, but also observe the high-resolution spin cycloid resonance (SCR) modes of a BFO single crystal in the temperature interval from 40 K to 300 K. The fine-splitting of the SCR modes is explained in terms of a microscopic model. The accurate measuring of spin harmonics of the spectroscopic SCR modes provides a sensitive probe of the easy-axis anisotropy in the BFO single crystal. Our findings can be valuable for future BFO devices, by using temperature or polarization as the external control parameters.

The BFO single crystal was grown in air using a Bi_2O_3–Fe_2O_3 high temperature flux technique. The as-grown crystals are millimeter sized black platelets. Electron microprobe analysis confirmed the stoichiometry of $BiFeO_3$. X-ray diffractometry measurements confirmed the sample to be rhombohedral BFO single crystal without detectable parasitic inclusions. High-quality crystal is indispensable for the reliable characterization of THz optical properties. In its ferroelectric phase (below $T_c \approx 1100$ K), BFO has a rhombohedrally distorted perovskite structure with the space group $R3c$ and lattice constants $a = 5.571$ Å and $c = 13.868$ Å at room temperature. As shown in Fig. 1(a), the spontaneous polarization $\boldsymbol{P}$ is along one of the pseudo-cubic [1, 1, 1] directions with a value between 50 μC/cm^2 and 100 μC/cm^2. Below $T_N \approx 640$ K, the cycloidal order develops along x'[1, 0, −1] for each (1, 1, 1) plane. These two directions define the (−1, 2, −1) cycloidal plane, where the spin rotation occurs, as shown in Figs. 1(a) and 1(b).

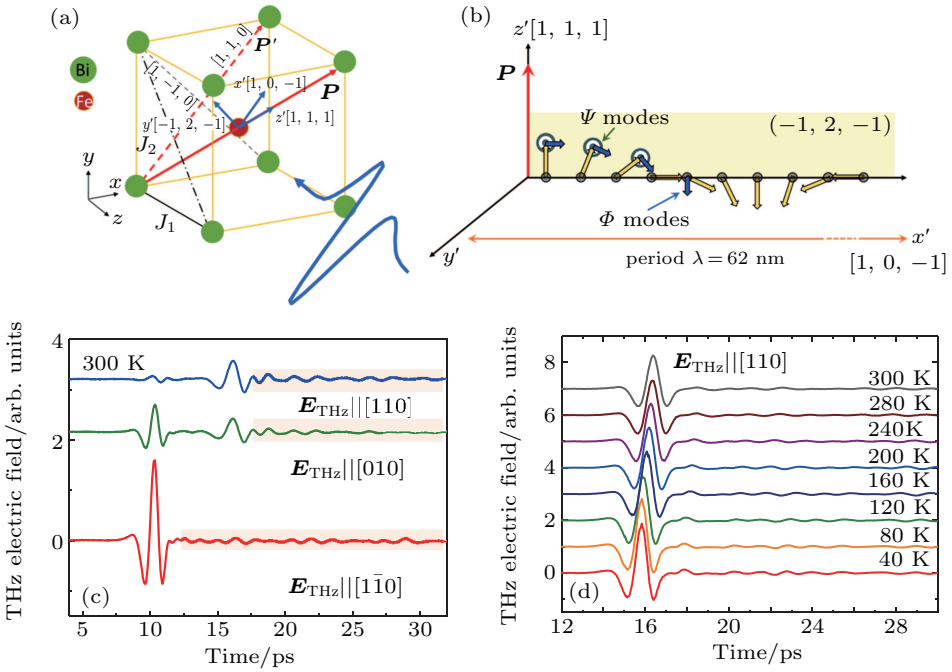


Fig. 1. (a) The structure of the pseudo-cubic BFO unit cell. The spontaneous polarization $\boldsymbol{P}$ is along the [111] direction. The spiral magnetic propagation is along the [1, 0, −1] direction. Geometry of THz transmission in BFO single crystal. (b) The cycloidal spatially modulated spins (vector $\boldsymbol{L}$) in the (−1, 2, −1) plane. Two species of spin excitations lie in and out of the cycloidal plane, respectively, corresponding to Φ and Ψ modes. (c) THz transmitted waveforms for $\theta = 0°$, 45°, 90° at room temperature. (d) The THz transients transmitted through the BFO crystal for $\theta = 0°$, which are shifted vertically according to different temperatures in the range of 40–300 K.

Our measurements were performed on a (001)-oriented BFO signal crystal, which was polished on both sides and had a thickness of $d = 0.652$ mm. We used a standard THz-TDS in transmission geometry to characterize the BFO crystal in the frequency range of 0.4–2 THz. The output of a mode-locked Ti:sapphire laser, with pulse duration 100 fs, central wavelength 800 nm, and repetition rate 80 MHz (MaiTai HP, Spectra-Physics), was used to generate and detect the THz transient. The generated THz pulses were collimated into parallel beams by a micro silicon lens. The sample was placed in a He flow cryostat mounted on an optical bench, and at the beam waist of the THz beam. The photoconductive switch consists of a metallic dipole antenna on a small piece of low-temperature (LT) grown GaAs with a sub-picosecond carrier lifetime. The photoinduced carriers of LT-GaAs are driven by the THz electromagnetic field, which produces a detected

current. The THz field amplitude is proportional to the current pulse. By a variable optical delay, the THz pulses generated at the emitter can be continuously delayed with respect to the gated detector, which allows us to temporally scan the electric fieldfor both the amplitude and the phase information. The THz-TDS system was purged with dry N_2 gas to reduce the THz absorption due to residual water vapor in the beam path.[30,31]

Figure 1(c) shows the THz transmitted waveforms as placing the BFO crystal in three different azimuth angles θ. The θ is defined as the angle between the incident electric-field of the THz pulse and the [1, 1, 0] direction, which is along the projection of the $\boldsymbol{P}$ on the (1,1,0) plane, $\boldsymbol{P}'$. THz waveforms recorded at $\theta = 0°$ ($\boldsymbol{E}_{\rm THz}||[1,1,0]$) and 90° ($\boldsymbol{E}_{\rm THz}||[1,-1,0]$) correspond to the ordinary (o-) and the extraordinary (e-) waves, respectively. When $\theta = 45°$ ($\boldsymbol{E}_{\rm THz}||[0,1,0]$), due to the strong anisotropy of BFO, the transmitted THz beam comprises two THz pulses, separated by approximately 6 ps with orthogonal polarization, while the amplitude is not exactly equal. The ratio of the peak amplitude of the o-wave to that of the e-wave gives the polarization state of the transmitted THz pulse. After the main part of the broadband THz pulse, the slowly decaying oscillation (as indicated by the shadow boxes) is caused by the long-wavelength SCR modes in BFO's cycloidal spin structure, as shown in Fig. 1(b) and will be discussed later. Figure 1(d) shows the transmitted THz waveforms with $\boldsymbol{E}_{\rm THz}||[1,1,0]$ measured at several selected temperatures. When the temperature is decreased, the time delay of the THz pulse is consequently decreased, which is due to the decrease of the group velocity of the THz pulses. Additionally, it can be found that the amplitude of the THz pulses increases with decreasing the temperature.

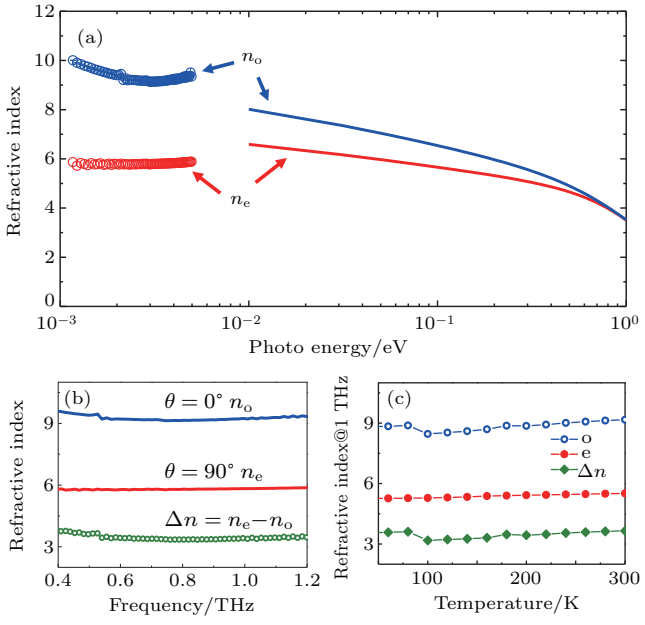


Fig. 2. (a) Photo energy and (b) THz frequency dependences of refractive index of BFO crystal for o- and e-THz waves. (c) n_o, n_e, and $\Delta n = n_o - n_e$ measured at 1 THz as a function of temperature.

The THz complex refractive index of the BFO crystal is extracted from the transmittance measurement at normal incidence, the details can be found in Ref. [32]. Figures 2(a) and 2(b) show the measured dispersion of n_e and n_o of the BFO crystal, in the photo energy and frequency domains, respectively. By using the plane-wave pseudopotential method based on density functional theory (DFT),[33] we calculate the n_o and n_e in the visible region, as shown by the solid lines in Fig. 2(a). In the calculation, the ion–electron interaction is modeled by the ultrasoft Vanderbilt-type pseudopotentials. For the sampling of the Brillouin zone, the electronic structures and optical properties use $3\times3\times2$ and $5\times5\times2$ k-point grids, respectively, generated according to the Monkhorst–Pack scheme. The experimental $BiFeO_3$ crystal structure with space group of $R3c$ and lattice parameters of $a = 5.57$ Å and $c = 13.87$ Å is adopted. It can be found that the birefringence of BFO increases with decreasing the photo energy. Within the 0.4–1.2 THz at room temperature, the optical birefringence of BFO is defined by $\Delta n = n_o - n_e = 3.65@1$ THz (n_e is smaller than n_o), which is much larger than that in the visible region around 0.34 (2.25 eV),[34] and $\Delta n = 1.6$–1.8 of $LiNbO_3$@1 THz (300 K).[35] Figure 2(c) shows a temperature-dependent anisotropic property. Far from the SCR resonances, Δn@1 THz decreases slightly from 3.65 at 300 K to about 3.18 at 100 K.

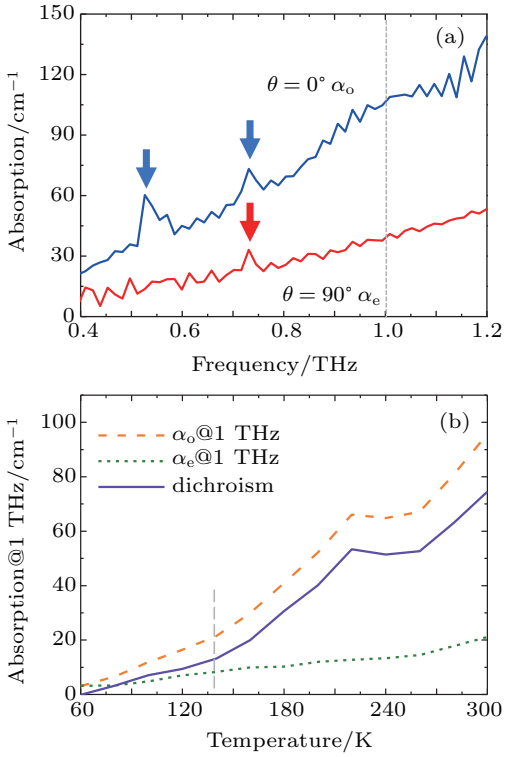


Fig. 3. (a) Frequency dependences of absorption coefficient of BFO crystal for o- and e-THz waves. (b) α_o, α_e, and $\Delta\alpha = \alpha_o - \alpha_e$ measured at 1 THz as functions of temperature.

Figure 3(a) shows the absorption coefficients of o- and e-waves, which are indeed increase with the increasing frequency. α_o is larger than α_e within the frequency range of

0.4–1.2 THz at room temperature. Although no phonons are expected in the present THz spectrum range, the broadband absorption at sub-THz frequencies originates from the broadening and softening of the phonon modes with increasing temperature. The lowest optical phonon of BFO is the E_g mode at 75 cm^{-1} ($\sim$ 2.25 THz).[36] It can also be found that the dichroism depends strongly on the temperature, as shown in Fig. 3(b). An increasing dichroism is observed at higher temperature, which can be attributed to the ferroelectric origin.[37–39] We conclude that the giant anisotropy suggests that the transverse phonons of E symmetry in BFO are strongly coupled to the THz electric field.

The dielectric tensor $\varepsilon(\boldsymbol{M},\boldsymbol{L})$ is a complex function of $\boldsymbol{M}$ and $\boldsymbol{L}$, where the ferromagnetic vector $\boldsymbol{M}=\boldsymbol{M}_1+\boldsymbol{M}_2$ and antiferromagnetic vector $\boldsymbol{L}=\boldsymbol{M}_1-\boldsymbol{M}_2$ for two sublattice magnetizations $\boldsymbol{M}_1$ and $\boldsymbol{M}_2$. In addition, figure 3(a) shows that the magnon resonance lines are superimposed over the absorption background, as highlighted by the arrows. They can be assigned to two families of spin waves, Φ and Ψ modes, indicating respectively the spins oscillating in and out of the plane of spin cycloid, as shown in Fig. 1(b). The in-plane cyclone mode has $\boldsymbol{m}_y$, $\boldsymbol{l}_z\neq 0$, while the out-of-plane mode has $\boldsymbol{m}_z$, $\boldsymbol{l}_y\neq 0$, where $\boldsymbol{m}$ and $\boldsymbol{l}$ are the dynamic components of $\boldsymbol{M}$ and $\boldsymbol{L}$, respectively.

Since Fishman *et al.* proposed a microscopic model in 2013, the spin state and microscopic spin-wave excitations of BFO are evaluated from the Hamiltonian which contains three components.[40–42] The first component is the exchange terms, which denote a sum over nearest neighbors (J_1) and next-nearest neighbors (J_2) on the pseudocubic lattice. The second component originates from the easy-axis anisotropy $\boldsymbol{K}$ along [1, 1, 1]. The third term contains two DM interactions. $\boldsymbol{D}$ along y' is responsible for the cycloidal period, while $\boldsymbol{D}'$ along z' produces the small tilt of the cycloid out of the $x'z'$ plane. The J_1 and J_2 determine the high-frequency part of the spin wave spectrum above 10 THz. The parameters $K=0.0035$ meV, $D=0.11$ meV, and $D'=0.054$ meV determine that the eigenfrequencies of the spin cycloid fall into the sub-THz range.[40–42] In the extended zone scheme with the modes in units of the cycloidal wave vector q, the excitations within the cycloidal plane have $\Phi_m=\Phi_1|m|$, which is a linear function of m. And the out-of-plane modes $\psi_m=\Phi_1\sqrt{1+m^2}$. Due to the higher harmonics of the cycloid generated by the competition of small tilting of the cycloid $\boldsymbol{D}'$ and the easy-axis anisotropy $\boldsymbol{K}$,[20,21,40] Φ_m and ψ_m ($m>0$) split into two modes labeled as $\Phi_m^{(1,2)}$ and $\psi_m^{(1,2)}$. As $m=0$, $\psi_0=\Phi_1$. Actually, ψ_0 and $\Phi_1^{(1)}$ are nearly degenerate for all $\boldsymbol{K}$ values. In addition, electromagnons are predicted in the incommensurate BFO spiral magnet by optical spectroscopy, due to the coupling between the spin waves and the electrical polarization.[17,43] All these theoretical predictions will be demonstrated by our THz experimental results in the following.

Figures 4(a) and 4(b)present the absorption spectra in the two polarizations at various temperatures, corresponding to $\boldsymbol{E}_{\rm THz}||[1,-1,0]$ and $\boldsymbol{E}_{\rm THz}||[1,1,0]$, which can be written as $\boldsymbol{h}_1=\left(\boldsymbol{x}'-\sqrt{3}\boldsymbol{y}'\right)/2$ and $\boldsymbol{h}_2=\boldsymbol{x}'/2+\sqrt{3}\boldsymbol{y}'/6+\sqrt{2/3}\boldsymbol{z}'$, respectively.[24,40] It should be mentioned that, we keep the time window just short of the first echo, which limits the maximum frequency resolution to be $\sim$ 0.033 THz ($\sim$ 1 cm^{-1}). Thus, the dielectric constants in this work are not modulated by any Fabry–Perot multiple inference, as mentioned in Ref. [22]. For the case of $\boldsymbol{E}_{\rm THz}||[1,1,0]$ ($\boldsymbol{h}_2$), there are four distinct absorption peaks clearly observed in the frequency range of 0.3–1 THz. Based on previous experimental data and theoretical works, we identify the SCR modes as follows. The resonance peak around 25 cm^{-1}@240 K is the Φ_2 mode. While the resonances peaks at 20 cm^{-1} and 18 cm^{-1}@240 K are assigned to the split of the $\psi_1^{(1,2)}$ mode. We note that $\psi_1^{(2)}$ is dominating in amplitude compared with the $\psi_1^{(1)}$ mode. With increasing temperature, the Φ_2 and $\psi_1^{(1,2)}$ modes display softening of the resonance frequencies. In addition, we also find a low frequency mode at frequencies around 10 cm^{-1}, which can be identified as $\Phi_1^{(2)}$, and is almost independent of the temperature.

As shown in Fig. 4(b), the absorption spectra measured with $\boldsymbol{E}_{\rm THz}||[1,-1,0]$ ($\boldsymbol{h}_1$) are observed to be different from the case of $\boldsymbol{E}_{\rm THz}||[1,1,0]$ We can distinguish five resonant lines in the case of $\boldsymbol{E}_{\rm THz}||[1,-1,0]$ ($\boldsymbol{h}_1$). Firstly, the resonance peaks around 25 cm^{-1}@240 K can also be observed for the Φ_2 mode. Our experimental data indicates that Φ_2 with the magnetic resonance (MR) component y' becomes spectroscopically active by both the fields of $\boldsymbol{h}_1$ and $\boldsymbol{h}_2$. Note that $\psi_1^{(2)}$ is completely absent, because $\psi_1^{(2)}$ with the MR component z' can only excited by the field $\boldsymbol{h}_2$. While $\psi_1^{(1)}$ with the MR component x' can be excited both by the fields $\boldsymbol{h}_1$ and $\boldsymbol{h}_2$. In addition, we observe low-frequency degenerate $\Phi_1^{(1)}$ and Ψ_0 modes with 15.7 cm^{-1}@60 K, which shift from 15.7 cm^{-1} to lower frequency 13.3 cm^{-1} when the sample temperature is increased. As shown by the squares in Fig. 4(b), it is interesting to note that a new mode at the frequency of $\sim$ 23.9 cm^{-1} (0.72 THz) appears when the temperature is lower than 140 K, which could be associated with a spin reorientation transition occurring around 140 K.[17,20,44] Similar magnon temperature dependence of rare-earth orthoferrites has been assigned to spin reorientation phase transition of the Fe^{3+} spin moments.[45] Our experimental data indicate a small spin reorientation out of the cycloidal plane (-1, 2, -1), as shown in Fig. 1(b). As shown in Fig. 3(b), an anomaly around 140 K in absorption properties suggests that this mode could be the electromagnon with both the magnetic and electrical dipole characters.

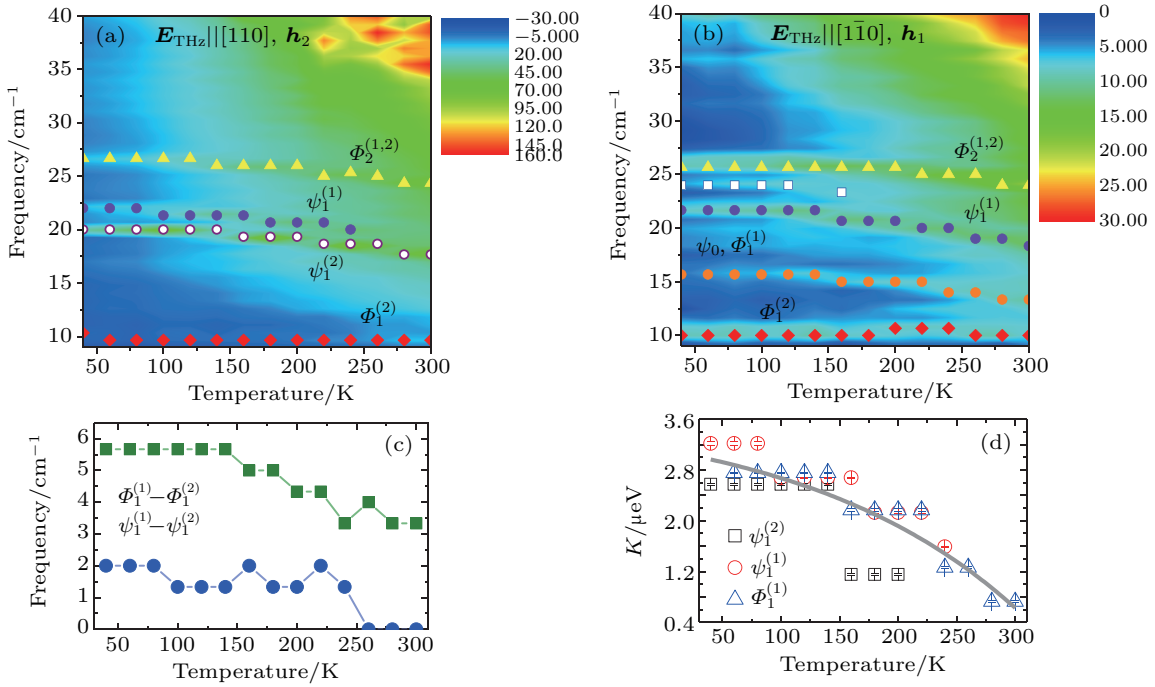


Fig. 4. (a), (b) The THz absorption coefficients in BFO as a function of frequency and temperature. (c) The splitting of $\psi_1^{(1,2)}$ mode and $\Phi_1^{(1,2)}$ mode. (d) Temperature dependence of the easy-axis anisotropy $\boldsymbol{K}$. The squares, circles, and triangles correspond to the data obtained for three modes, for varying temperatures. The solid line is guide for the eyes.

According to our two cases of polarization dependent measurement, the ordinary ray shows the splitting of $\psi_1^{(1,2)}$ mode; the extraordinary ray shows the splitting of $\Phi_1^{(1,2)}$ mode. Figure 4(c) plots the splits of $\psi_1^{(1,2)}$ and $\Phi_1^{(1,2)}$ modes: $\Delta\psi_1 = \psi_1^{(1)} - \psi_1^{(2)}$ and $\Delta\Phi_1 = \Phi_1^{(1)} - \Phi_1^{(2)}$, as functions of temperature. The splitting of $\psi_1^{(1,2)}$ and $\Phi_1^{(1,2)}$ results from not only the easy-axis anisotropy $\boldsymbol{K}$ along the [1, 1, 1] direction of the electric polarization $\boldsymbol{P}$, but also the additional DM interaction $\boldsymbol{D}'$ along [1, 1, 1]. Following the temperature dependent frequencies of spin-wave modes $\psi_1^{(1,2)}$ and $\Phi_1^{(1)}$ in BFO, figure 4(d) shows the calculated values of easy-axis anisotropy $\boldsymbol{K}$ as a function of temperature, with the DM interaction parameter of $D' = 54$ μeV.[40,41]

In conclusion, we reported THz-frequency optical constants of BFO as a function of temperature, for polarizations along two crystallographic directions of [1, 1, 0] and [1, −1, 0]. We observed that a refractive index difference between n_o and n_e can reach 3.6 between 0.4 and 1.2 THz. The temperature-dependent giant anisotropy of BFO crystal in the THz region can be attributed to the phonon mode. The distinct SRC modes are reliably detected in the temperature range of 40–300 K. To account for our results, we applied a microscopic model of Fishman *et al.*, the magnon peaks are assigned as the in-plane Φ_2, $\Phi_1^{(1,2)}$ modes, and the out-of-plane two $\psi_1^{(1,2)}$ modes. The easy-axis anisotropy has been determined experimentally by the spin harmonics of the cycloid. The THz-optical properties of a BFO single crystal will lay the groundwork for the spectral and technological applications[46–48] of this important multiferroic material.

References

[1] Spaldin N A and Ramesh R 2019 *Nat. Mater.* **18** 203
[2] Eerenstein W, Mathur N D and Scott J F 2006 *Nature* **442** 759
[3] Cheng Z X, Wang X L, Du Y and Dou S X 2010 *J. Phys. D: Appl. Phys.* **43** 242001
[4] Catalan G and Scott J F 2009 *Adv. Mater.* **21** 2463
[5] Sosnowska I, Neumaier T P and Steichele E 1982 *J. Phys. C* **15** 4835
[6] You L, Zheng F, Fang L, Zhou Y, Tan L Z, Zhang Z Y, Ma G H, Schmidt D, Rusydi A, Wang L, Chang L, Rappe A M and Wang J L 2018 *Sci. Adv.* **4** 3438
[7] Choi T, Lee S, Choi Y J, Kiryukhin V and Cheonget S W 2009 *Science* **324** 63
[8] Kundys B, Viret M, Colson D and Kundys D O 2010 *Nat. Mater.* **9** 803
[9] Jin Z, Xu Y, Zhang Z, Lin X, Ma G, Cheng Z and Wang X 2012 *Appl. Phys. Lett.* **101** 242902
[10] Ruello P, Ruello P, Pezeril T, Avanesyan S, Vaudel G, Gusev V, Infante I C and Dkhil B 2012 *Appl. Phys. Lett.* **100** 212906
[11] Jin Z, Xu Y, Zhang Z, Li G, Lin X, Ma G, Cheng Z and Wang X 2012 *Appl. Phys. Lett.* **100** 071105
[12] Kumar A, Rai R C, Podraza N J, Denev S, Ramirez M, Chu Y H, Martin L W, Ihlefeld J, Heeg T, Schubert J, Schlom D G, Orenstein J, Ramesh R, Collins R W, Musfeldt L J and Gopalan V 2008 *Appl. Phys. Lett.* **92** 121915
[13] Talbayev D, Lee S, Cheong S W and Taylor A J 2008 *Appl. Phys. Lett.* **93** 212906
[14] Takahashi K, Kida N and Tonouchiet M 2006 *Phys. Rev. Lett.* **96** 117402
[15] Matsuda M, Fishman R S, Hong T, Lee C H, Ushiyama T, Yanagisawa Y, Tomioka Y and Ito T 2012 *Phys. Rev. Lett.* **109** 067205
[16] Jeong J, Goremychkin E A, Guidi T, Nakajima K, Jeon G S, Kim S A, Furukawa S, Kim Y B, Lee S, Kiryukhin V, Cheong S W and Park J G 2012 *Phys. Rev. Lett.* **108** 077202
[17] Cazayous M, Gallais Y, Sacuto A, Sousa R, Lebeugle D and Colson D 2008 *Phys. Rev. Lett.* **101** 037601
[18] Rovillain P, Cazayous M, Gallais Y, Sacuto A, Lobo R P S M, Lebeugle D and Colson D 2009 *Phys. Rev. B* **79** 180411
[19] Fishman R S, Lee J H, Bordács S, Kézsmárki I, Nagel U and Rõõm T 2015 *Phys. Rev. B* **92** 094422
[20] Gaikwad V M and Acharya S A 2013 *J. Appl. Phys.* **114** 193901
[21] Ruette B, Zvyagin S, Pyatakov A P, Bush A, Li J F, Belotelov V I, Zvezdin A K and Viehland D 2004 *Phys. Rev. B* **69** 064114

[22] Caspers C, Gandhi V P, Magrez A, Rijk E and Ansermet J P 2016 *Appl. Phys. Lett.* **108** 241109
[23] Białek M, Ito T, Rønnow H and Ansermet J P 2019 *Phys. Rev. B* **99** 064429
[24] Talbayev D, Trugman S A, Lee S, Yi H T, Cheong S W and Taylor A J 2011 *Phys. Rev. B* **83** 094403
[25] Kézsmárki I, Nagel U, Bordács S, Fishman R S, Lee J H, Yi H T, Cheong S W and Rõõm T 2015 *Phys. Rev. Lett.* **115** 127203
[26] Chen F, Goodfellow J, Liu S, Grinberg I, Hoffmann M C, Damodaran A R, Zhu Y, Zalden P, Zhang X, Takeuchi I, Rappe A M, Martin L W, Wen H and Lindenberg A M 2015 *Adv. Mater.* **27** 6371
[27] Liu X, Zhang Z, Lin X, Zhang K, Jin Z, Cheng Z and Ma G 2016 *Opt. Express* **24** 26618
[28] Feng H J, Yang K, Deng W, Li M, Wang M, Duan B, Liu F, Tian J and Guo X 2015 *Phys. Chem. Chem. Phys.* **17** 26930
[29] Guzelturk B, Mei A B, Zhang L, Tan L Z, Donahue P, Singh A G, Schlom D G, Martin L W and Lindenberg A 2020 *Nano Lett.* **20** 145
[30] Jepsen P U, Cooke D G and Koch M 2011 *Laser Photon. Rev.* **5** 124
[31] Ulbricht R, Hendry E, Shan J, Heinz T F and Bonn M 2011 *Rev. Mod. Phys.* **83** 543
[32] Li J G, Yang S M, Chen X, Zhuang N F, Zhu Q B, Wu A H, Lin X, Ma G H, Jin Z M and Yao J Q 2019 *Chin. Phys. Lett.* **36** 044203
[33] Yaakob M K, M F M Taib M F M, Lu L, Hassan O H and Yahya M Z A 2015 *Mater. Res. Express* **2** 116101
[34] Rivera J P and Schmid H 1997 *Ferroelectrics* **204** 23
[35] Sun Y M, Mao Z L, Hou B H, Liu G Q and Wang L 2007 *Chin. Phys. Lett.* **24** 414
[36] Kamba S, Nuzhnyy D, Savinov M, Šebek J, Petzelt J, Prokleška J, Haumont R and Kreisel J 2007 *Phys. Rev. B* **75** 024403
[37] Seizi N, Naoki T, Hideaki K, Mitsuo W T and Seiji K 2002 *Phys. Med. Biol.* **47** 3771
[38] Masato S, Noriaki K, Sachio H and Hiroshi O 2015 *ACS Photon.* **2** 1373
[39] Mavrona E, Chodorow U, Barnes M E, Parka J, Palka N, Saitzek S, Blach J F, Apostolopoulos V and Kaczmarek M 2015 *AIP Adv.* **5** 077143
[40] Fishman R S, Furukawa N, Haraldsen J T, Matsuda M and Miyahara S 2012 *Phys. Rev. B* **86** 220402
[41] Fishman R S 2013 *Phys. Rev. B* **87** 224419
[42] Fishman R S, Haraldsen J, Furukawa N and Miyahara S 2013 *Phys. Rev. B* **87** 134416
[43] Chen H B and Li Y Q 2013 *Appl. Phys. Lett.* **102** 252906
[44] Singh M, Katiyar R and Scott J 2008 *J. Phys.: Condens. Matter* **20** 252203
[45] Jin Z M, Ruan S Y, Li J G, Lin X, Ren W, Cao S X, Ma G H and Yao J Q 2019 *Acta Phys. Sin.* **68** 167501 (in Chinese)
[46] Chen L, Liao D G, Guo X G, Zhao J Y, Zhu Y M and Zhuang S L 2019 *Front. Inform. Technol. Electron. Eng.* **20** 591
[47] Feng H J, Wang M, Duan B, Tian J and Guo X 2015 *J. Alloys Compd.* **628** 311
[48] Wehmeier L, N€orenberg T, Oliveira T V A G, Klopf J M, Yang S Y, Martin L W, Ramesh R, Eng L M and Kehr S C 2020 *Appl. Phys. Lett.* **116** 071103